Title

Water oxidation catalysis via immobilization of the dimanganese complex [Mn 2 (μ-O) 2 Cl(μ-O 2 CCH 3)(bpy) 2 (H 2 O)](NO 3) 2 onto silica

Journal

Dalton Transactions, 42(34)

ISSN

1477-9226

Authors

Rumberger, Evan MW

Ahn, Hyun S

Bell, Alexis T

et al.

Publication Date

2013

DOI

10.1039/c3dt51472b

Peer reviewed

Dalton Transactions

RSC Publishing

PAPER

View Article Online
View Journal | View Issue

Cite this: *Dalton Trans.*, 2013, **42**, 12238

Water oxidation catalysis *via* immobilization of the dimanganese complex $[Mn_2(\mu\text{-}O)_2Cl(\mu\text{-}O_2CCH_3)(bpy)_2(H_2O)](NO_3)_2$ onto silica†

Evan M. W. Rumberger,[a,b] Hyun S. Ahn,[a,b] Alexis T. Bell*[a,b] and T. Don Tilley*[a,b]

Adsorption of a dinuclear μ-oxo bridged Mn complex onto mesoporous silica was observed when SBA15 was treated with an acetonitrile solution of $[Mn_2(\mu\text{-}O)_2Cl(\mu\text{-}O_2CCH_3)(H_2O)(bpy)_2](NO_3)_2$ (**1**). This complex was immobilized *via* the displacement of NO_3^- into solution, and characterization by spectroscopic (DRIFTS and DRUV-vis) and magnetic data indicates that the intact dication is electrostatically bound to the silica surface. Loadings of up to 4.1% by weight of $[Mn_2(\mu\text{-}O)_2Cl(\mu\text{-}O_2CCH_3)(H_2O)(bpy)_2]^{2+}$ were achieved. TEM images of the grafted material revealed retention of the mesoporous structure of SBA15, and no clusters of manganese greater than *ca.* 10 nm were observed. The SBA15-supported dimanganese complex functions as a catalyst for the oxidation of H_2O with $(NH_4)_2Ce(NO_3)_6$ as stoichiometric oxidant. In contrast, homogenous aqueous solutions of **1** do not evolve oxygen upon treatment with $(NH_4)_2Ce(NO_3)_6$. Labeling studies with $H_2{}^{18}O$ confirm that the oxygen formed in this catalysis is derived from water. Monitoring the O_2 evolution allowed determination of an initial rate for the catalysis (TOF_i = 1.1×10^{-3} s^{-1}). These studies also reveal a first order dependence on manganese surface concentration, and a zero order rate dependence for $(NH_4)Ce(NO_3)_6$. Spectroscopic investigations were employed to investigate the difference in activities between dissolved and supported dimanganese complexes.

Received 3rd June 2013,
Accepted 10th July 2013

DOI: 10.1039/c3dt51472b

www.rsc.org/dalton

Introduction

The development of inexpensive materials that might serve as catalysts for the oxidation of water to O_2 has been the goal of many investigations.[1–11] Biological systems responsible for photosynthesis accomplish this task by use of a tetranuclear μ-oxo bridged manganese center as the oxygen-evolving complex (OEC) in photosystem II (PSII).[12–20] The OEC catalyzes the four-electron oxidation of water to molecular oxygen according to eqn (1).

$$2H_2O \rightarrow O_2 + 4H^+ + 4e^- \quad (1)$$

The mechanism by which PSII carries out this process is complex and not yet fully understood,[21–23] but it is believed that a highly oxidized state of the cluster is directly involved in water oxidation. Numerous model complexes have been synthesized to help elucidate the reaction pathways governing water oxidation at PSII,[24] and these range from dinuclear to tetranuclear clusters. However, only a few have been reported to exhibit activity for water oxidation catalysis.[25–47] More recently, inorganic molecular analogues of the active site of PSII, including a calcium atom in the μ-oxo bridged cluster, has been synthesized by Agapie and coworkers.[42,43] However, the catalytic activity of these compounds is yet to be determined.

A convenient screening method for evaluation of catalytic activity for water oxidation involves addition of a Ce(IV) salt in the presence of water.[48] Such Ce(IV) species (typically, $(NH_4)_2Ce(NO_3)_6$) serve as outer-sphere oxidants for potential catalytic species. The observation of oxygen evolution for a Ce(IV)-promoted oxidation of water was first reported for manganese catalysts by Kaneko *et al.*, for the dinuclear complexes $[(bpy)_2Mn^{III}O_2Mn^{IV}(bpy)_2]^{3+}$ and $[(phen)_2Mn^{III}O_2Mn^{IV}(phen)_2]^{3+}$.[28] These complexes exhibited very low activities, about 0.8 turnovers after 4 h, perhaps due to the lack of an open coordination site for water. Kaneko *et al.* observed that $[Mn^{III}(salen)H_2O](ClO_4)$ decomposed in the presence of Ce(IV) to yield an insoluble material which evolved oxygen in aqueous solutions.[32] Crabtree, Brudvig and coworkers have studied oxygen-evolving processes involving the mixed-valent dinuclear complex $[(H_2O)(terpy)Mn^{IV}O_2Mn^{III}(terpy)(H_2O)]^{3+}$, using NaOCl or $KHSO_5$ as the oxygen atom donors.[37,38] For these reactions, a reactive Mn=O intermediate was invoked.[39]

[a]*Departments of Chemistry and Chemical Engineering, University of California at Berkeley, Berkeley, California 94720, USA*
[b]*Chemical Sciences Division, Lawrence Berkeley National Laboratory, 1 Cyclotron Road, Berkeley, California 94720, USA. E-mail: tdtilley@berkeley.edu, bell@cchem.berkeley.edu*

†Electronic supplementary information (ESI) available. See DOI: 10.1039/c3dt51472b

Interestingly, Yagi and Narita[25] reported catalytic evolution of O_2 from the same manganese complex, after it was adsorbed onto Kaolin clay and treated with $(NH_4)_2Ce(NO_3)_6$. Isotopic ^{18}O labeling studies showed that the evolved O_2 was unambiguously derived from H_2O. No oxygen evolution was observed for homogeneous aqueous solutions of this complex. The catalyst structure; however, did not appear to survive the adsorption and the mixed-valent Mn(IV)–Mn(III) complex was found to oxidize upon immobilization to form a Mn(IV) species of unknown composition. In a subsequent study, Yagi and coworkers investigated the reactivity of the same complex after adsorption onto mica.[26] Catalytic O_2 evolution was again observed but the identity of the catalyst after adsorption was not established. Recent work by Spiccia and coworkers has demonstrated a similar phenomenon, that spatial confinement of Mn(II) precursors in the channels of Nafion generated small manganese oxide particles, surface sites of which resemble the active site of PSII.[41] Thus, whereas several immobilized manganese catalysts derived from molecular precursors lack thorough characterization, immobilization appears to offer a promising design element for water oxidation catalysis, especially given the fact that it is employed in nature.

This investigation was designed to probe the influence of immobilization on the catalytic activity of manganese complexes towards water oxidation. The targeted molecule is the dinuclear Mn(IV) complex $[Mn_2(\mu\text{-}O)_2Cl(\mu\text{-}O_2CCH_3)(H_2O)(bpy)_2](NO_3)_2$ (**1**), first reported by Christou and coworkers.[49] This complex seemed to possess several properties of interest, including the relatively high oxidation state ($Mn^{IV}Mn^{IV}$) and the $Mn_2(\mu\text{-}O)_2$ fragment in common with the active site of PSII. Such a d^3/d^3 core should be relatively inert toward ligand substitution, and this could contribute to catalyst stability. In addition, the acetate bridge was expected to help stabilize the Mn_2O_2 fragment. Finally, the presence of an aquo ligand seemed essential for redox processes that could cycle through $Mn\text{–}OH_2$ to Mn=O transformations.

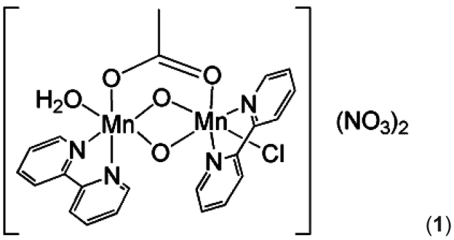

(**1**)

To our knowledge, there are no literature reports of a thoroughly characterized Mn complex that retains its structure after immobilization onto a heterogeneous solid support, and exhibits activity for water oxidation. Here we report the results of a study in which the dinuclear μ-oxo bridged Mn complex **1** was supported onto mesoporous SBA15 silica. Characterization of the supported complex by a number of techniques indicates that immobilization occurs by an ion-exchange reaction resulting in electrostatic binding of the cation of **1** to the silica surface. Silica-supported **1** revealed modest catalysis for water oxidation, although **1** is inactive in homogenous aqueous solution under analogous conditions.

Results

Synthesis and characterization of Mn_2-SBA15 (2)

The catalyst adsorption onto silica was accomplished by stirring an acetonitrile solution of **1** with the suspended support material at room temperature for 16 h. Over this time, the green-brown color of **1** dissipates from solution, as the insoluble SBA15 takes on this same color. The grafting of complex **1** onto SBA15 was monitored by UV-visible spectroscopy (Fig. 1). The UV-visible spectrum of **1** in acetonitrile solution exhibited three important features. A sharp intense peak was observed at ~200 nm and was assigned to the NO_3^- counter ion of complex **1** based on observation of a similar peak in the spectrum of a solution of $NaNO_3$. A medium intensity peak was observed at 300 nm. This absorption was assigned to the bpy ligand based on comparison with the spectrum of a solution of bpy. A broad, medium intensity absorption, typically seen in Mn(IV) oxo-bridged dimers,[50–57] was observed in the 300–500 nm region and was assigned to a $[Mn_2O_2]^{4+}$ LMCT. A relatively low intensity absorption, also attributed to a $[Mn_2O_2]^{4+}$ LMCT,[51,52] was observed at 650 nm.

Acetonitrile solutions of **1** were found to obey the Beer–Lambert law (by monitoring the concentration dependence of the peak at 300 nm). A comparison of the UV-visible spectrum of a 0.96 mM acetonitrile solution of **1** (15 mL pregraft solution) with that obtained by mixing this solution with a 15 mL acetonitrile slurry of SBA15 (postgraft solution) revealed that the peak at 300 nm lost intensity after the mixture had been stirred for 16 h. The loss in intensity at 300 nm corresponds to adsorption of 73% of the starting complex **1** onto the SBA15. Notably, this grafting procedure did not result in a significant loss of NO_3^- from solution (by UV-vis spectroscopy), indicating

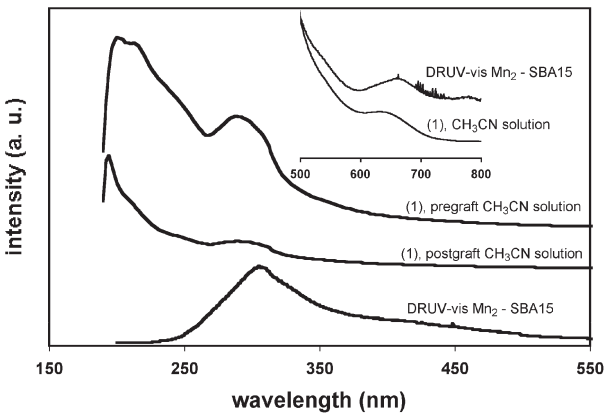

Fig. 1 UV-visible spectrum (top trace) of a CH_3CN solution of complex **1**. Solution UV-visible (middle trace) of a CH_3CN solution of complex **1** 16 h after being added to a CH_3CN slurry of SBA15. Diffuse reflectance spectra (bottom trace) of Mn_2-SBA15 (**2**). The inset is a magnification of the 500–800 nm region.

that only the cationic species $[Mn_2(\mu\text{-}O)_2Cl(\mu\text{-}O_2CCH_3)(H_2O)(bpy)_2]^{2+}$ is absorbed onto SBA15. Manganese weight loadings were determined by Mn ICP analysis of the isolated materials. Materials with different $[Mn_2(\mu\text{-}O)_2Cl(\mu\text{-}O_2CCH_3)(H_2O)(bpy)_2]^{2+}$ weight loadings (0.58–4.14%) were synthesized by varying the concentration of **1** in the acetonitrile pregraft solution. The maximum loading of 4.14% corresponds to a surface coverage of 0.05 molecules of $[Mn_2(\mu\text{-}O)_2Cl(\mu\text{-}O_2CCH_3)(H_2O)(bpy)_2]^{2+}$ per square nanometer of SBA15 surface area. For comparison, the SBA15 (BET surface area 684 $m^2\ g^{-1}$) initially possessed an OH coverage of 1.7 nm^{-2}.

Diffuse reflectance UV-vis (DRUV-vis) spectra (Fig. 1, lower trace) collected for Mn_2-SBA15 corroborated the assertion that complex **1** was adsorbed onto the SBA15 as $[Mn_2(\mu\text{-}O)_2Cl(\mu\text{-}O_2CCH_3)(H_2O)(bpy)_2]^{2+}$. The absorbance at 200 nm attributed to the NO_3^- is absent in the DRUV-vis spectrum collected for the Mn_2-SBA15; however, the other UV active chromophore (at 300 nm) of the $[Mn_2(\mu\text{-}O)_2Cl(\mu\text{-}O_2CCH_3)(H_2O)(bpy)_2]^{2+}$ unit were observed for the immobilized complex.

TEM images of Mn_2-SBA15 (**2**) were collected to determine whether or not nanometer-scale particles of MnO_x, or another type of Mn-based cluster, was present on the support after grafting (Fig. S1†). TEM images confirmed that the hexagonal pore structure of the SBA15 remained intact after the grafting of **1** and that Mn-containing nanoparticles $\geq$*ca.* 10 nm did not form in the pores of the support. Low-angle PXRD experiments verified that the mesoporous SBA15 structure persisted through the grafting procedure. An intense peak observed at $2\theta = 0.97°$ is assigned to (001) reflections resulting from the long range hexagonal pore structure of SBA15. Crystalline manganese oxides were not observed in wide-angle PXRD measurements. Adsorption of complex **1** onto SBA15 had a minimal effect on both the surface area and pore volume distribution of the material (Fig. S2†). Isotherms of IUPAC classification type IV were observed for the Mn_2-SBA15 material. The narrow pore size distribution of the SBA15 (Fig. S2,† inset) remained essentially unperturbed after complex **1** was adsorbed.

DRIFTS spectra of Mn_2-SBA15 (**2**) present additional evidence that **1** had adsorbed onto SBA15 as $[Mn_2(\mu\text{-}O)_2Cl(\mu\text{-}O_2CCH_3)(H_2O)(bpy)_2]^{2+}$. The peak assignments given in Fig. 2 were made with reference to literature values, and to spectra for the isolated complex.[49] The difference spectrum derived from spectra of SBA15 and Mn_2-SBA15 clearly exhibits bands corresponding to the acetate and bpy ligands of **1**. This spectrum does not contain peaks for NO_3^-, indicating that this species is not present on the surface. In addition, loss of intensity for the absorbances corresponding to isolated Si–OH (3745 cm^{-1}) and hydrogen bonded Si–OH (2800–3700 cm^{-1}) groups of SBA15 (not shown in Fig. 2) indicates that **1** grafts onto the silica surface by cation exchange of $[Mn_2(\mu\text{-}O)_2Cl(\mu\text{-}O_2CCH_3)(H_2O)(bpy)_2]^{2+}$ with silanol protons.

Several lines of evidence indicate that complex **1** interacts with the surface of silica *via* a cation-exchange reaction which leads to electrostatic binding of the intact $[Mn_2(\mu\text{-}O)_2Cl(\mu\text{-}O_2CCH_3)(H_2O)(bpy)_2]^{2+}$ to the surface (Scheme 1). This is also supported by chemical tests that verified the presence of Cl^- in Mn_2-SBA15 (**2**) (see Experimental section). However, the data described above does not indicate whether or not the $Mn_2(\mu\text{-}O)_2$ dinuclear core of this dication remains intact after cation exchange. The presence of this $Mn_2(\mu\text{-}O)_2$ fragment should be reflected in the magnetic properties of the supported complex.

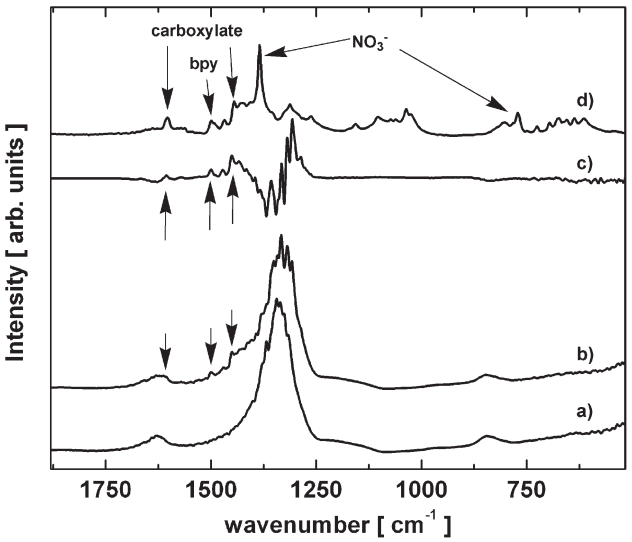

Fig. 2 DRIFTS spectra (a) of SBA15 before treatment with an acetonitrile solution of complex **1**. DRIFTS spectra (b) of SBA15 after treatment with an acetonitrile solution of complex **1**. Transmission FT-IR (spectrum d) of a KBr pelletized sample of complex **1**. DRIFTS (c) difference spectra of Mn_2-SBA15 (**2**) and SBA15. See the text for a discussion of the peak assignments.

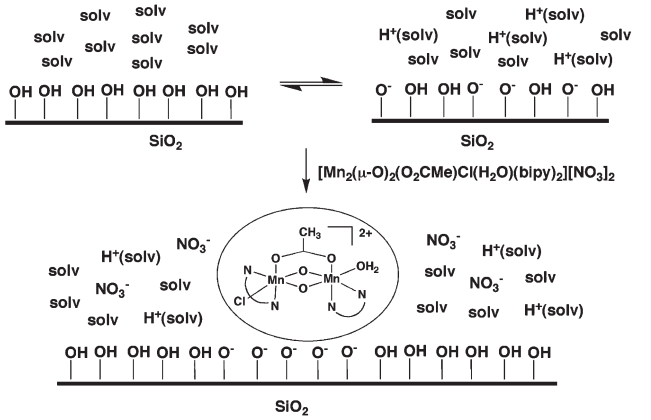

Scheme 1 Grafting of **1** on SBA-15.

Magnetic properties of supported $[Mn_2(\mu\text{-}O)_2Cl(\mu\text{-}O_2CCH_3)(H_2O)(bpy)_2]^{2+}$

The magnetic properties of the unsupported precursor **1** were reported by Christou and coworkers.[49] The observed antiferromagnetic exchange[58] interactions propagate through the bridging oxo and acetate ligands that link the two Mn(IV) ($S = 3/2$) nuclei within the $Mn_2(\mu\text{-}O)_2$ dinuclear core. Fig. S3† shows variable-temperature DC magnetic susceptibility data collected

for Mn_2-SBA15 in the temperature range of 100–300 K with an applied field of 1 T. The diamagnetic contribution of SBA15 was measured and subtracted from the Mn_2-SBA15 susceptibilities to yield paramagnetic quantities for the supported complex. The measured properties are listed in Table S1.† The temperature dependence of the magnetic susceptibility for **2** is antiferromagnetic as indicated by the decrease in the magnetic moment, $\chi_M T$, with decreasing temperature. The room temperature magnetic moment (2.2 cm^3 K mol^{-1}) of the Mn_2-SBA15 material is the same as that of the precursor complex **1** and is much lower than that expected for two non-interacting Mn(IV) ions (7.5 cm^3 K mol^{-1}). The agreement of the room temperature magnetic moment of Mn_2-SBA15 and the precursor complex **1** strongly suggests that the complex remains intact upon grafting, but this data does not exclude the presence of closely related dimeric Mn(IV) complexes exhibiting similar magnetic behavior.

The data for $\chi_M T$ *versus* temperature were least squares-fit to a theoretical model in order to ascertain the magnitude of the magnetic exchange interaction. The exchange interactions were represented with an isotropic spin Hamiltonian with theoretical susceptibilities calculated from a least-squares fit of the experimental data to the Van Vleck equation (see ESI† for details). The results of the analysis are listed in Table S1.† The *g*- and *J*-values measured for Mn_2-SBA15 are in good agreement with those observed for the precursor complex **1**. However, the *J*-value (−29 cm^{-1}) obtained for the Mn_2-SBA15 is slightly less negative than what was seen for complex **1** (−36 cm^{-1}). This deviation is likely the result of a small distortion in the $[Mn_2O_2]^{4+}$ moiety. It is possible that the interaction of the $[Mn_2(\mu\text{-}O)_2Cl(\mu\text{-}O_2CCH_3)(H_2O)(bpy)_2]^{2+}$ unit with a surface bound siloxide or hydrogen bonded silanol could change the Mn–O–Mn angle enough to sufficiently account for this minor difference in the *J*-value. Despite this small difference, it is important to emphasize that a value of $J = -29$ cm^{-1} falls within the expected range of values for Mn_2O_2 type complexes in which both Mn atoms are in the 4+ oxidation state.[58]

Oxygen evolution studies

A 0.0078 g sample of Mn_2-SBA15 (**2**) was treated with 1.5 mL of a 200 mM solution of $(NH_4)_2Ce(NO_3)_6$, and the resulting evolution of O_2 was monitored with a Clark electrode (Fig. 3). The water used for this experiment had previously been sparged with N_2 for 30 min. Oxygen evolution was monitored until the oxygen concentration reached about 80% of its saturation level in solution. Near the O_2 saturation level, the electrode response data became erratic, presumably because of O_2 bubble formation at the membrane of the Clark electrode. At a reaction time of 6.8 min, the yield of oxygen was 75% (based on catalyst loading), which represented 78% of the oxygen saturation level. The turnover frequency (TOF) reached a maximum at 30 s, with a value of 4.5×10^{-3} s^{-1}, and then slowly declined over the following 7 min to a value of 1.5×10^{-3} s^{-1}. After 2 h, aliquots of the reaction solution did not contain MnO_4^- or leached complex **1**, as indicated by UV-visible spectroscopy. For comparison, a similar experiment with analogous conditions was conducted with an aqueous solution of **1** and $(NH_4)_2Ce(NO_3)_6$. As shown in Fig. 3, this solution did not evolve oxygen over the course of 7 min. Thus, the adsorption of **1** onto a SBA15 solid support is necessary for the stabilization or activation of **1** as a catalyst for water oxidation. Catalytic water oxidation was observed when a 0.206 g portion of Mn_2-SBA15 was treated with 8 mL of a 200 mM solution of $(NH_4)_2Ce(NO_3)_6$ and allowed to stir for 16 h at room temperature. After this time, 1.5 mL of O_2, which corresponds to 4.4 turnovers, had evolved.

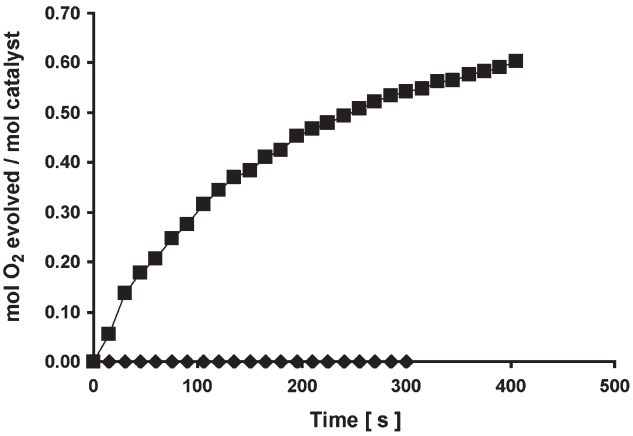

Fig. 3 Oxygen evolution of Mn_2-SBA15 (squares), and complex **1** (diamond) in 200 mM Ce(IV) water solution (1.5 mL).

The surface concentration of **1** on SBA-15 was varied from 1.64–3.93 wt% in order to investigate whether surface-immobilized complex **1** is operating in a single-site fashion or collectively with other sites through surface migration and/or agglomeration. Fig. 4 shows that the TOF observed was similar for all surface manganese loadings, and this indicates that the Mn_2-SBA15 catalysts are operating in a "single site" mode, with independently functioning catalytic surface sites.

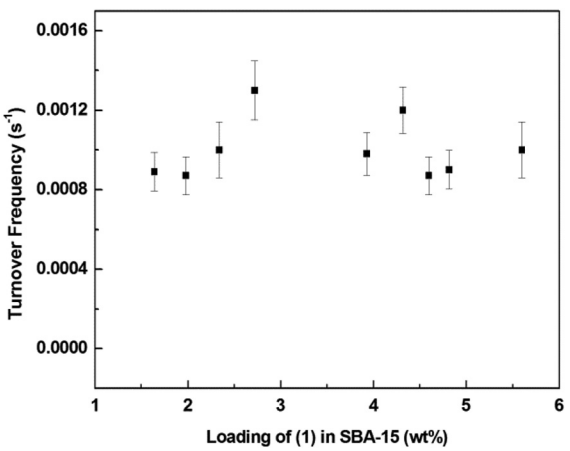

Fig. 4 Water oxidation TOF plotted against surface concentration of complex **1** in 200 mM Ce(IV) water solution (1.5 mL).

Table 1 Summary of the isotopic compositions of evolved oxygen in ^{18}O-labeling experiments

	$H_2{}^{18}O$–H_2O v/v %	$^{16}O_2$	$^{16}O^{18}O$	$^{18}O_2$	Φ_{18O}%
Measured evolved O_2	10.2 ± 2.6	83.7 ± 3.8	13.4 ± 3.3	2.5 ± 0.6	9.6 ± 2.2
Statistical distribution		80.5 ± 2.1	18.4 ± 0.5	1.0 ± 0.03	10.2 ± 2.6

^{18}O-labeling studies

To establish the source of oxygen in the oxygen evolution experiments, ^{18}O labeled H_2O was used and the gas evolved was analyzed by mass spectrometry. A dinitrogen-purged flask was charged with 0.1607 g of **2** along with a 10.2% $H_2{}^{18}O$–H_2O v/v enriched 200 mM $(NH_4)_2Ce(NO_3)_6$ solution at 23 °C. After allowing this solution to stir for 16 h, gas samples (0.75 mL) were collected from the headspace (10 mL) and then injected into a mass spectrometer for isotope analysis, by monitoring peaks at m/z = 32 ($^{16}O_2$), 34 ($^{16}O^{18}O$), and 36 ($^{18}O_2$). The findings are summarized in Table 1. For 10.2% $H_2{}^{18}O$–H_2O v/v enriched water, the total isotopic fraction (Φ_{18O}) of the evolved O_2 (Φ_{18O} = 9.6 ± 2.2) matched that of the starting water solvent (Φ_{18O} = 10.2), indicating that water was the sole source of the evolved O_2. Control experiments using unlabeled H_2O and ambient laboratory "air" samples did not produce m/z = 34 or 36 peaks quantifiable above the baseline.

Kinetic studies

Initial rates of O_2 evolution were measured to determine the reaction orders of cerium oxidant and Mn_2 catalyst. Measurements of the kinetics of O_2 evolution were monitored at 23 °C using a Clark electrode. The reaction order in catalyst was determined by measuring the O_2 evolution rates under conditions for which the Ce(IV) concentrations were held constant while varying the $[Mn_2(\mu\text{-}O)_2Cl(\mu\text{-}O_2CCH_3)(H_2O)(bpy)_2]^{2+}$ catalyst loadings. The reaction order in Ce(IV) was determined by varying the concentration of Ce(IV) (2–524 equiv. relative to moles of $[Mn_2(\mu\text{-}O)_2Cl(\mu\text{-}O_2CCH_3)(H_2O)(bpy)_2]^{2+}$) and monitoring the O_2 evolution rate for a given catalyst loading. As depicted in Fig. 5, initial rates (r_I, mol g^{-1} s^{-1}) of O_2 evolution exhibit a linear response with respect to catalyst loading (measured for 0.5–4.1 wt% $[Mn_2(\mu\text{-}O)_2Cl(\mu\text{-}O_2CCH_3)(H_2O)(bpy)_2]^{2+}$), indicating a first-order dependence of the Mn_2-supported dimer for water oxidation. The plot of log r_I *versus* the log of catalyst concentration gave a straight line with a slope of 1 (inset, Fig. 5), verifying the first order dependence on Mn catalyst concentration. On the other hand, cerium exhibited a zero-order dependence, as illustrated in Fig. 6. These experiments provided the empirical rate law, rate = $k_{obs}[Mn_2]$, where $k_{obs} = 1.1 \times 10^{-3}$ s^{-1}.

Stability of 1 in water

Aqueous solutions of complex **1** were observed to change color rapidly from brownish green to red within a few minutes of their preparation. A similar situation was not, however, observed for acetonitrile solutions of **1**. Therefore, it was of interest to examine the stability of **1** in aqueous solutions in the absence of an oxidizing reagent. This effort was further motivated by a study by Baffert and coworkers,[59] in which it was observed that aqueous solutions (pH = 4–5, 0.1 M KO_3SCF_3) of $[Mn^{III/IV}{}_2O_2(terpy)_2(OH_2)_2]^{3+}$ decomposed upon electrochemical oxidation, *via* rapid deprotonation and condensation to a tetramanganese complex (eqn (2)). The process was monitored by UV-visible spectroscopy, which showed that conversion of aquo to oxo ligands is accompanied by formation of a linear oxo, Mn^{IV}–O–Mn^{IV} bridge giving rise to a broad absorption between 400 and 500 nm.[59]

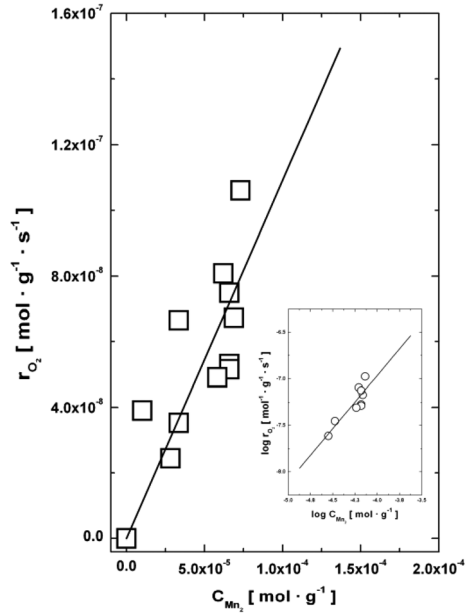

Fig. 5 Initial rate of O_2 evolution plotted *versus* molar quantity of Mn_2 catalyst. The same Ce(IV) concentration of 300 mM was used for each measurement.

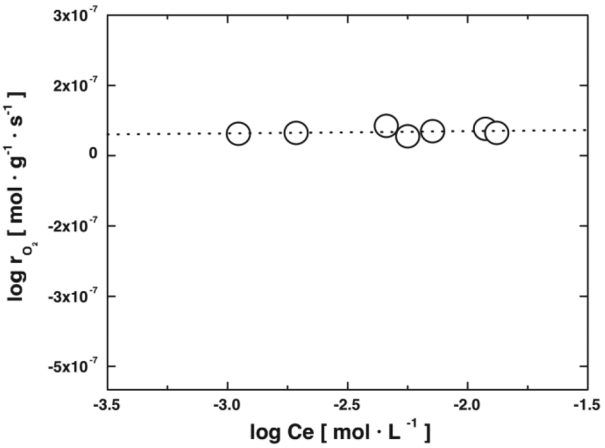

Fig. 6 Logarithm of the initial rate of O_2 evolution plotted *versus* the log of Ce (IV) concentration. The same material with a catalyst loading of 3.52 wt% $[Mn_2O_2Cl(O_2CCH_3)(bpy)(H_2O)]^{2+}$ was used in each measurement.

$$2\,[(H_2O)(terpy)Mn^{IV}(\mu\text{-}O)_2Mn^{III}(terpy)(H_2O)]^{3+}$$

$$\downarrow \; -2e^-$$

$$2\,[(H_2O)(terpy)Mn^{IV}(\mu\text{-}O)_2Mn^{IV}(terpy)(H_2O)]^{3+}$$

$$\downarrow \; -2H^+, -H_2O$$

$$[(H_2O)(terpy)_2Mn^{IV}(\mu\text{-}O)_2Mn^{IV}(\mu\text{-}O)Mn^{IV}(\mu\text{-}O)_2Mn^{IV}(terpy)_2(H_2O)]^{6+} \quad (2)$$

Fig. 7a shows the growth of an absorbance between 375 nm and 550 nm for an unbuffered, aqueous solution of **1** (10^{-6} M) over the course of 1 h. This behavior closely follows that observed by Baffert and coworkers for 0.1 M KO_3SCF_3 aqueous solutions of $[(H_2O)(terpy)Mn^{IV}O_2Mn^{III}(terpy)(H_2O)]^{3+}$. Thus, it appears that the coordinated water ligand of **1** is readily converted to a μ-oxo tetra manganese complex in solution. The latter complex could not be isolated, but a DRIFTS spectrum of the material that precipitates from aqueous solutions of **1** contains a band at 808 cm^{-1} (Fig. S4†), assigned as a linear μ-oxo Mn^{IV}–O–Mn^{IV} bridging stretch based on numerous literature precedents and ^{18}O labeling studies.[69–72]

Consistent with this chemistry, the observed transformations are pH sensitive, as determined by monitoring buffered solutions of **1** by UV-vis spectroscopy, and the decomposition is more rapid under more basic conditions. Fig. 7b illustrates the spectra collected for complex **1** (10^{-6} M) in a pH = 9.6 sodium carbonate/sodium bicarbonate buffered solution. An immediate color change to red was observed for complex **1** dissolved in this basic solution. Within 12 min of the initial UV-visible scan, a band had grown in the region of 375–550 nm that was equivalent in intensity to that seen after 36 min in the unbuffered solution. The UV-visible spectra of an acetic acid/sodium acetate buffered solution (pH = 4.5) of **1** exhibited no evidence for decomposition over 60 min, as seen in Fig. 7c. Aqueous solutions of **1** were found to be acidic; an 8 mM aqueous solution of **1** had a measured pH of 2.3. This solution was titrated with a 50 mM solution of NaOH to determine the equivalence point. It was found that three mols of the NaOH titrant per one mol of complex **1** were required to reach the equivalence point. Two acidic protons of **1** might originate from the coordinated aquo ligand, while a third might come from a protonated μ-O ligand. The proposed decomposition of **1** in aqueous solution is illustrated in eqn (3).

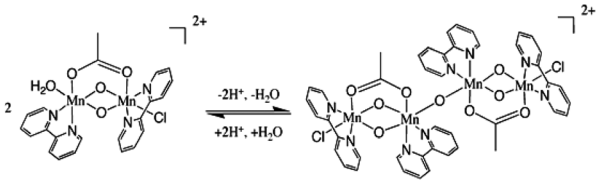

(3)

It is noteworthy that the coordinated water ligand of complex **1** appears to be replaced by a bridging linear oxo ligand in the aqueous decomposition product. Such a complex should not be active as a water oxidation catalyst, since it possesses no binding site for water. It would then follow that if complex **1** is to catalyze water oxidation *via* an intermediate having a M=O moiety, then the oxo ligand resulting from successive deprotonations of the coordinated water must be stabilized against deactivating dimerization reactions. Indeed, when the presumably tetrameric manganese species isolated from the aqueous solution of **1** was subjected to water oxidation conditions, no oxygen evolution was observed. Surface immobilization of the tetrameric species onto SBA-15 also resulted

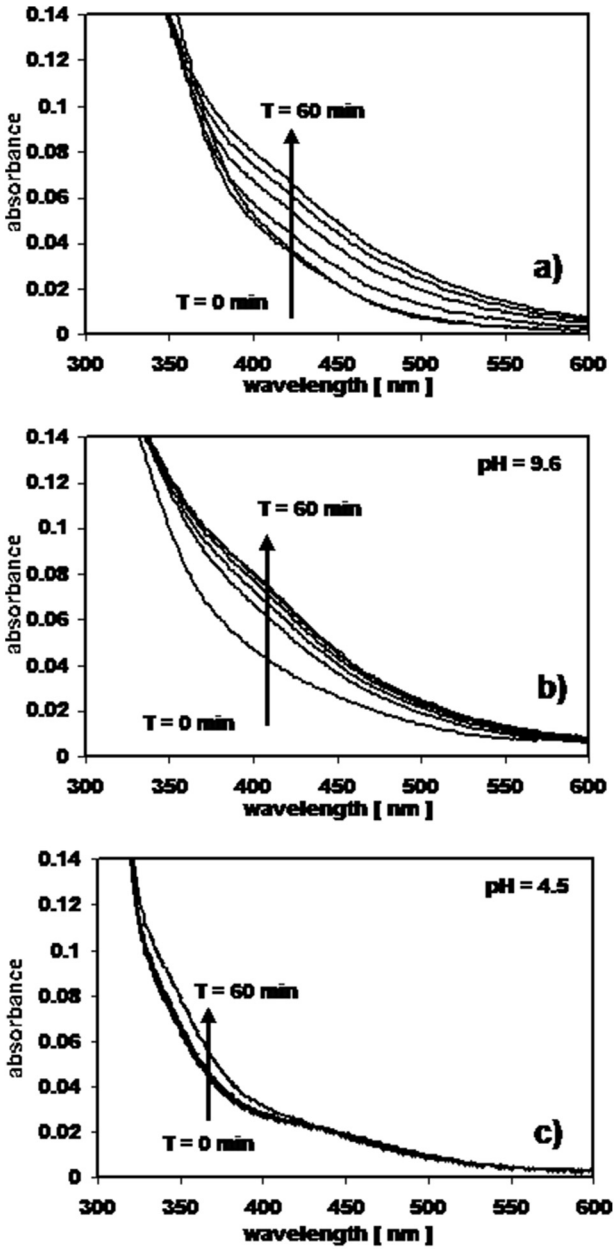

Fig. 7 UV-visible spectra collected for a 10^{-6} M solutions of complex **1** for (a) unbuffered solution, (b) a pH = 9.6 buffered solution, and a (c) acetic acid/sodium acetate pH = 4.5 buffered solution. Measurements were performed at 12-minute intervals.

in an inactive catalyst, further suggesting that the loss of the coordinated water ligand and subsequent dimerization is a decomposition pathway that prevents water oxidation catalysis.

Stability of Mn_2-SBA15 (2) in water

The stability of Mn_2-SBA15 (**2**) in water was also examined. A 0.010 g portion of **2** was dispersed in 1 mL of water. The resulting greenish brown slurry was allowed to stand undisturbed at room temperature for 24 h in a sealed vial. After 24 h, there was no observable color change of the slurry. The slurry was then allowed to air dry at room temperature over a period of 16 h. Fig. S5† illustrates the DRUV-visible spectrum of **2** recorded before (trace labeled (a) in Fig. S5†) and after the water exposure (trace labeled (b) in Fig. S5†). As can be seen in Fig. S5,† all of the UV-vis features observed for the dry Mn_2-SBA15 material, including the $[Mn_2O_2]^{4+}$ LMCT at 650 nm, persist after water exposure. The acetate and bpy ligands are still observed in DRIFTS spectra collected for Mn_2-SBA15 after the water-exposure.

Stability of Mn_2-SBA15 (2) when treated with Ce(IV) solutions

Fig. S6† compares the diffuse reflectance spectrum of Mn_2-SBA15 with that of a Mn_2-SBA15 sample that was treated with a 200 mM solution of $(NH_4)_2Ce(NO_3)_6$ for 16 h. The treated catalyst was washed five times with 20 mL of distilled water and air dried before the spectrum was recorded. As shown in Fig. S6,† this treatment gives rise to a significant, broad absorbance in the region between 350 and 700 nm. This new peak could be due to new species possessing linear Mn–O–Mn linkages, and/or adsorbed Ce(IV) oxidant which also exhibits a strong absorption in this region.[60,61] It is likely that the cationic dimeric catalyst is displaced from the surface by the large excess of Ce(IV) or Ce(III) in solution, but Mn decomposition products may also reabsorb onto the silica support. Thus, the modest number of turnovers observed (4.4) can be attributed to cationic exchange of the grafted complex with Ce(III) or Ce(IV) into solution, and the accompanying catalyst decomposition.

Discussion

The results presented above demonstrate that the dimanganese complex **1** is readily adsorbed onto the mesoporous SBA15 silica support. Vibrational and electronic spectroscopies show that the adsorption process involves immobilization of the intact cation of **1**, $[Mn_2(\mu\text{-}O)_2Cl(\mu\text{-}O_2CCH_3)(H_2O)(bpy)_2]^{2+}$, onto the silica surface. While the magnetic data suggests a small difference between the structures of the supported and unsupported dication, the bulk of the evidence indicates that the dication is largely unperturbed upon immobilization onto silica, and that the interaction with the surface is primarily electrostatic. This immobilization stabilizes the dication toward dimerization/oligomerization processes, and this is perhaps the reason why the heterogeneous material, Mn_2-SBA15 (**2**), catalyzes water oxidation whereas homogeneous solutions of **1** do not.

This study suggests that immobilization may be a key requirement for the development of active catalysts for water oxidation. Indeed, nature employs this strategy in the OEC of PSII, in which the manganese cluster involved in water splitting is immobilized in a membrane. This effect of immobilization on water oxidation catalysis has also been reported by Yagi and Narita for the dimanganese species $[Mn_2(\mu\text{-}O)_2(terpy)_2(OH_2)_2]^{3+}$, although the exact nature of the resulting surface-bound catalyst has not yet been determined.[25,26] The observed chemistry of **1** and $[Mn_2(\mu\text{-}O)_2(terpy)_2(OH_2)_2]^{3+}$ in aqueous solution[58] provides a reasonable explanation for this requirement. A water molecule that is coordinated to the metal center of a catalyst will not function as a bridging ligand. However, the water oxidation process likely transforms the aquo ligand into hydroxo (M–OH), and then oxo (M=O), ligands that may greatly prefer a bridging environment (M–OH–M or M–O–M). Thus, manganese catalysts are rapidly deactivated in solution. It seems clear that immobilization represents a potentially useful strategy for catalyst synthesis that may allow examination of structure–activity relationships for a wide range of manganese-based water oxidation catalysts. The study described here indicates that electrostatic binding of the catalyst to silica is insufficient for providing a long-lived, active catalyst, since the operating conditions employed led to competing decomposition (and probable leaching) of the catalyst.

The limited number of published kinetic studies for the Ce(IV) oxidation of water with Mn-based catalysts prevents a broad comparison of catalyst activities with Mn_2-SBA15 (**2**). The most detailed study available for comparison is the report of Yagi and Narita, who examined the activity of $[Mn_2(\mu\text{-}O)_2(terpy)_2(OH_2)_2]^{3+}$ immobilized on mica and kaolin.[26] For these catalysts, the rate of O_2 evolution was found to have a second-order dependence on catalyst loading. The authors proposed a bimolecular process whereby an intermolecular coupling of two Mn^V=O moieties constitute the O–O bond-forming step. The activity of Mn_2-SBA15 compares favorably to the catalyst examined by Yagi and Narita, having a rate constant approximately twice as large (k_{obs} = 1.1 × 10^{-3} s^{-1} for **2** *vs.* k_{obs} = 0.48 × 10^{-3} s^{-1} for $[Mn_2(\mu\text{-}O)_2(terpy)_2(OH_2)_2](NO_3)_3$ adsorbed on mica under optimal catalyst loading conditions).

A possible mechanism for water oxidation, as catalyzed by Mn_2-SBA15 (**2**), is proposed in Scheme 2. Step A involves oxidation of the surface bound dication of **1**, which results in loss of protons from the coordinated water ligand and formation of an oxidized Mn dimer. If not for immobilization, the latter species would likely agglomerate *via* formation of additional Mn–O–Mn linkages. The oxidation of Mn_2-SBA15 (**2**) must occur rapidly to be consistent with the observed zero-order dependence on the $(NH_4)_2Ce(NO_3)_6$ concentration.

The oxidized Mn complex resulting from step A is described with two resonance structures, one involving a Mn(V)=O oxo species and the other described as a Mn(IV) oxyl radical. A contribution from the latter structure is suggested by theoretical studies, which proposes that this type of structure may form *via* oxidative deprotonation of the manganese complex

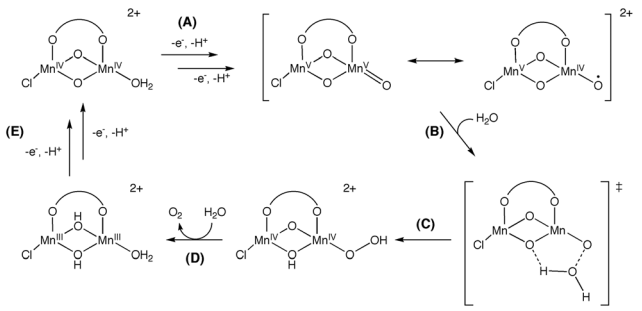

Scheme 2 Proposed water oxidation cycle by **1** on SBA-15.

$[(H_2O)(terpy)Mn^{IV}O_2Mn^{III}(terpy)(H_2O)]^{3+}$.[62–64] These calculations also suggest that the high oxidation state manganese oxo complex may be nucleophilically attacked by a water molecule (or hydroxide anion), *via* a hydrogen-bonded transition state, to produce a hydroperoxy intermediate (steps B, C). Similar transition states have been proposed for catalase mimics based on Mn dimeric complexes.[65,66] A water molecule, as opposed to hydroxide, is the preferred nucleophile given the acidic reaction conditions used in the oxygen evolution experiments (pH < 1). Step D involves the elimination of oxygen with formation of a reduced, hydroxo-bridged dimanganese center, which would then be oxidized to complete the catalytic cycle.

Conclusions

The immobilization of $[Mn_2(\mu\text{-}O)_2Cl(\mu\text{-}O_2CCH_3)(bpy)(H_2O)]^{2+}$ onto silica leads to an active catalyst for water oxidation The exact nature of the catalytically active species has not been firmly established, but spectroscopy, kinetic data and loading studies suggest that the active sites are independent Mn_2 units that are structurally similar to the dicationic complex. Furthermore, deactivation of this system seems to be associated with the formation of μ-OH and μ-O linkages resulting from water activation. While no spectroscopic evidence for an active Mn=O species was obtained in this study, the aqueous decomposition products observed by the UV-vis experiments indicate that a coordinated H_2O ligand at manganese is a necessary ingredient for water oxidation to proceed. In this particular system, spectroscopic monitoring of the functioning active site is complicated by the competing condensation of dimanganese species on the surface, which is made possible by the mode of immobilization (electrostatic binding).

Experimental section

General

All reactions were performed under an inert atmosphere using standard Schlenk techniques. Acetonitrile was distilled from phosphorous pentoxide and stored under a dry nitrogen atmosphere. The dinuclear Mn complex, $[Mn_2(\mu\text{-}O)_2Cl(\mu\text{-}O_2CCH_3)(H_2O)(bpy)_2](NO_3)_2$ (**1**), was synthesized using a published procedure and its purity was verified by elemental analysis and FT-IR spectroscopy.[49] Solution UV-vis spectra were collected with HP 8452A Series 3000 and Varian Cary 300 series spectrophotometers. Solution UV-vis spectra were collected with acetonitrile as the solvent. FT-IR spectra were collected on Nicolet 300 and Mattson Instruments Galaxy 3000 series spectrometers equipped with a Pike Technologies EasyDiff diffuse reflectance accessory. Magnesium oxide and potassium bromide were used as white standards for diffuse reflectance UV-vis and DRIFTS measurements, respectively. Magnetic measurements were performed on a Quantum Design MPMS-7 magnetometer equipment with a 7 Tesla superconducting magnet. Diamagnetic contributions from the sample holder were subtracted from the collected data. Surface area measurements were performed by the BET method as implemented by a Quantachrome Autosorb-1 surface area analyzer. SBA15 surface hydroxyl group densities were measured by an NMR titration method[67] using $Mg(CH_2Ph)_2(THF)_2$; reported values correspond to an average of two results, which always agreed to within 15%. TEM data were collected with a Tecnai G2 20 transmission electron microscope (FEI) at 200 kV beam acceleration. Samples for TEM studies were prepared by deposition of a hexane suspension of the catalyst material onto carbon-coated copper obtained from Ted Pella, Inc. Oxygen evolution was monitored at 23 °C using a YSI 5331 Clark style electrode. A MKS Minilab mass spectrometer was used for isotope analysis. Head space gas samples (typically 0.75 mL) were collected with a gas tight syringe and injected into a 110 °C He flow which was sampled by the mass spectrometer. It was assumed that the response factors for ^{18}O-containing fragments were identical to those of the corresponding ^{16}O-containing fragments. Stock solutions of 99.0% ^{18}O $H_2{}^{18}O$ were purchased from Cambridge Isotope Laboratories, Inc. ICP elemental analysis (manganese) was performed by Galbraith Laboratories, Inc. and on a Perkin-Elmer ICP-OES Optima 7000 DV at the college of chemistry facility at the University of California, Berkeley.

Materials

The mesoporous silica, SBA15, was synthesized using a literature method.[68] The calcined material was dried under a dynamic vacuum while being heated to 250 °C for 16 h. The dried material was stored under a dry N_2 atmosphere. The surface area and average pore radius of the SBA15 were measured with BET N_2 sorption and were found to be 684 $m^2\ g^{-1}$ and 25 Å respectively. The hydroxyl group concentration was determined to be 1.7 OH nm^{-2}.

Mn_2-SBA15 (2)

In a typical preparation, the following procedure was used. A 25 mL acetonitrile slurry of SBA15 (1.16 g) was treated with a deep brown/green acetonitrile solution (25 mL) of $[Mn_2(\mu\text{-}O)_2Cl(\mu\text{-}O_2CCH_3)(H_2O)(bpy)_2](NO_3)_2$ (**1**) (0.050 g) under a dry N_2 atmosphere, resulting in a slow bleaching of the solution while the color of the complex (green) was transferred to the SBA15. The resulting material was isolated by filtration

after allowing the slurry to stir for 16 hours. The Mn_2-SBA15 material was thoroughly washed three times (3 × 15 mL) with acetonitrile. The resultant green/brown material, Mn_2-SBA15 (**2**), was dried at 60 °C for 16 h under a dynamic vacuum.

Chloride test

To a 20 mL solution made from 10 mL of concentrated nitric acid and 10 mL of water was added 0.0204 g of the Mn_2-SBA15 material. The yellow turbid solution was allowed to stir for 2 hours, followed by filtration through a glass frit. A 10 mL water solution containing 0.5 g of silver nitrate was slowly added over a period of 5 minutes. A milky precipitate of silver chloride was immediately observed. A control experiment with SBA15 did not yield a silver chloride precipitate.

Acknowledgements

This work was supported by the Director, Office of Science, Office of Basic Energy Sciences of the US Department of Energy under contract no. DE-AC02-05CH11231.

Notes and references

1 M. Yagi and M. Kaneco, *Chem. Rev.*, 2001, **101**, 21.
2 R. Eisenberg and D. G. Nocera, *Inorg. Chem.*, 2005, **44**, 6799.
3 J. H. Alstrum-Acevedo, M. K. Brennaman and T. J. Meyer, *Inorg. Chem.*, 2005, **44**, 6802.
4 P. G. Hoertz and T. E. Mallouk, *Inorg. Chem.*, 2005, **44**, 6828.
5 M. Grätzel, *Inorg. Chem.*, 2005, **44**, 6841.
6 G. J. Meyer, *Inorg. Chem.*, 2005, **44**, 6852.
7 S. Chakraborty, T. J. Wadas, H. Hester, R. Schmehl and R. Eisenberg, *Inorg. Chem.*, 2005, **44**, 6865.
8 J. L. Dempsey, A. J. Esswein, D. R. Manke, J. Rosenthal, J. D. Soper and D. G. Nocera, *Inorg. Chem.*, 2005, **44**, 6879.
9 A. J. Nozik, *Inorg. Chem.*, 2005, **44**, 6893.
10 N. S. Lewis, *Inorg. Chem.*, 2005, **44**, 6900.
11 O. Kruse, J. Rupprecht, J. R. Mussgnug, G. C. Dismukes and B. Hankamer, *Photochem. Photobiol. Sci.*, 2005, **4**, 957.
12 R. D. Britt, J. M. Peloquin and K. A. Campbell, *Annu. Rev. Biophys. Biomol. Struct.*, 2000, **29**, 463.
13 B. A. Diner and F. Rappaport, *Annu. Rev. Plant Biol.*, 2002, **53**, 551.
14 J. P. McEvoy and G. W. Brudvig, *Chem. Rev.*, 2006, **106**, 4455.
15 K. N. Ferreira, T. M. Iverson, K. Maghlaoui, J. Barber and S. Iwata, *Science*, 2004, **303**, 1831.
16 B. Loll, J. Kern, W. Saenger, A. Zouni and J. Biesiadka, *Nature*, 2005, **438**, 1040.
17 J. Yano, J. Kern, K. Sauer, M. Latimer, Y. Pushkar, J. Biesiadka, B. Loll, W. Saenger, J. Messinger, A. Zouni and V. K. Yachandra, *Science*, 2006, **314**, 821.
18 K. Sauer and V. K. Yachandra, *Biochim. Biophys. Acta, Bioenerg.*, 2004, **1655**, 140.
19 V. K. Yachandra, *Philos. Trans. R. Soc. London, Ser. B*, 2002, **357**, 1347.
20 V. K. Yachandra, K. Sauer and M. P. Klein, *Chem. Rev.*, 1996, **96**, 2927.
21 J. P. McEvoy, J. A. Gascon, V. S. Batista and G. W. Brudvig, *Photochem. Photobiol. Sci.*, 2005, **4**, 940.
22 J. P. McEvoy and G. W. Brudvig, *Phys. Chem. Chem. Phys.*, 2004, **6**, 4754.
23 V. L. Pecoraro and W.-Y. Hsieh, in *Manganese and Its Role in Biological Processes*, ed. A. Sigel and H. Sigel, Marcel Dekker Inc., New York, 2000, vol. 37, pp. 429–504.
24 S. Mukhopadhyay, S. K. Mandal, S. Bhaduri and W. H. Armstrong, *Chem. Rev.*, 2004, **104**, 3981.
25 M. Yagi and K. Narita, *J. Am. Chem. Soc.*, 2004, **126**, 8084.
26 K. Narita, T. Kuwabara, K. Sone, K. Shimizu and M. Yagi, *J. Phys. Chem. B*, 2006, **110**, 23107.
27 A. K. Poulsen, A. Rompel and C. J. McKenzie, *Angew. Chem., Int. Ed.*, 2005, **44**, 6916.
28 R. Ramaraj, A. Kira and M. Kaneko, *Angew. Chem., Int. Ed. Engl.*, 1986, **25**, 825.
29 R. Ramaraj, A. Kira and M. Kaneko, *Chem. Lett.*, 1987, 261.
30 T. Matsushita, M. Fujiwara and T. Shono, *Chem. Lett.*, 1981, 631.
31 Y. Naruta, M. Sasayama and T. Sasaki, *Angew. Chem., Int. Ed. Engl.*, 1994, **33**, 1839.
32 K. V. Gobi, R. Ramaraj and M. Kaneko, *J. Mol. Catal.*, 1993, **81**, L7.
33 K. Narita, T. Kuwabara, K. Sone, K. Shimizu and M. Yagi, *J. Phys. Chem. B*, 2006, **110**, 23107.
34 Y. Shimazaki, T. Nagano, H. Takesue, B.-H. Ye, F. Tani and Y. Naruta, *Angew. Chem., Int. Ed.*, 2004, **43**, 98.
35 H. Chen, T. Ranitendranath, G. Olack, J. Vrettos, T.-C. Weng, J. Penner-Hahn, R. H. Crabtree and G. W. Brudvig, *Inorg. Chem.*, 2006, **46**, 34.
36 D. L. Howard, A. D. Tinoco, G. W. Brudvig, J. S. Vrettos and B. C. Allen, *J. Chem. Educ.*, 2005, **82**(5), 791.
37 J. Limburg, J. S. Vrettos, L. M. Liable-Sands, A. L. Rheingold, R. H. Crabtree and G. W. Brudvig, *Science*, 1999, **283**, 1524.
38 J. Limburg, J. S. Vrettos, M. N. Collomb, L. M. Liable-Sands, A. L. Rheingold, R. H. Crabtree and G. W. Brudvig, *J. Inorg. Biochem.*, 1999, **74**, 207.
39 J. Limburg, J. S. Vrettos, H. Y. Chen, J. C. de Paula, R. H. Crabtree and G. W. Brudvig, *J. Am. Chem. Soc.*, 2001, **123**, 423.
40 R. Tagore, H. Chen, H. Zhang, R. H. Crabtree and G. W. Brudvig, *Inorg. Chim. Acta*, 2007, **360**, 2983.
41 R. K. Hocking, R. Brimblecombe, L. Chang, A. Singh, M. H. Cheah, C. Glover, W. H. Casey and L. Spiccia, *Nat. Chem.*, 2011, **3**, 461.
42 J. S. Kanady, E. Y. Tsui, M. W. Day and T. Agapie, *Science*, 2011, **333**, 733.
43 E. Y. Tsui, R. Tran, J. Yano and T. Agapie, *Nat. Chem.*, 2013, **5**, 293.

44 D. J. Wasylenko, R. D. Palmer and C. P. Berlinguette, *Chem. Commun.*, 2013, **49**, 218.
45 K. J. Young, L. A. Martini, R. L. Milot, R. C. Snoeberger III, V. S. Batista, C. A. Schmuttenmaer, R. H. Crabtree and G. W. Brudvig, *Coord. Chem. Rev.*, 2012, **256**, 2503.
46 X. Liu and F. Wang, *Coord. Chem. Rev.*, 2012, **256**, 1115.
47 H. Dau, L. Christian, T. Reier, M. Risch, S. Roggan and P. Strasser, *ChemCatChem*, 2010, **2**, 724.
48 V. Nair and V. Deepthi, *Chem. Rev.*, 2007, **107**, 1862.
49 S. Bhaduri, A. J. Tasiopoulos, M. A. Bolcar, K. A. Abboud, W. E. Streib and G. Christou, *Inorg. Chem.*, 2003, **42**, 1483.
50 H. J. Mok, J. A. Davis, S. Pal, S. K. Mandal and W. H. Armstrong, *Inorg. Chim. Acta*, 1997, **263**, 385.
51 D. R. Gamelin, M. L. Kirk, T. L. Stemmler, S. Pal, W. H. Armstrong, J. E. Pennerhahn and E. I. Solomon, *J. Am. Chem. Soc.*, 1994, **116**, 2392.
52 T. C. Brunold, D. R. Gamelin, T. L. Stemmler, S. K. Mandal, W. H. Armstrong, J. E. Penner-Hahn and E. I. Solomon, *J. Am. Chem. Soc.*, 1998, **120**, 8724.
53 M. L. Kirk, M. K. Chan, W. H. Armstrong and E. I. Solomon, *J. Am. Chem. Soc.*, 1992, **114**, 10432.
54 S. Pal and W. H. Armstrong, *Inorg. Chem.*, 1992, **31**, 5417.
55 S. Pal, M. M. Olmstead and W. H. Armstrong, *Inorg. Chem.*, 1995, **34**, 4708.
56 S. Pal, J. W. Gohdes, W. C. A. Wilisch and W. H. Armstrong, *Inorg. Chem.*, 1992, **31**, 713.
57 T. H. Parsell, R. K. Behan, M. T. Green, M. P. Hendrich and A. S. Borovik, *J. Am. Chem. Soc.*, 2006, **128**, 8728.
58 N. A. Law, J. W. Kampf and V. L. Pecoraro, *Inorg. Chim. Acta*, 2000, **297**, 252.
59 C. Baffert, S. Romain, A. Richardot, J. C. Lepretre, B. Lefebvre, A. Deronzier and M. N. Collomb, *J. Am. Chem. Soc.*, 2005, **127**, 13694.
60 H. L. Greenhaus, A. M. Feibush and L. Gordon, *Anal. Chem.*, 1957, **29**, 1531.
61 A. I. Medalia and B. J. Byrne, *Anal. Chem.*, 1951, **23**, 453.
62 G. Aullón, E. Ruiz and S. Alvarez, *Chem.–Eur. J.*, 2002, **8**, 2508.
63 P. E. M. Siegbahn, *Inorg. Chem.*, 2000, **39**, 2923.
64 M. Lundberg, M. R. A. Blomberg and P. E. M. Siegbahn, *Inorg. Chem.*, 2004, **43**, 264.
65 M. U. Triller, H. Wen-Yuan, V. L. Pecoraro, A. Rompel and B. Krebs, *Inorg. Chem.*, 2002, **41**, 5544.
66 A. J. Wu, J. E. Penner-Hahn and V. L. Pecoraro, *Chem. Rev.*, 2004, **104**, 903.
67 K. L. Fujdala and T. D. Tilley, *J. Am. Chem. Soc.*, 2001, **123**, 10133.
68 D. Y. Zhao, Q. S. Huo, J. L. Feng, B. F. Chmelka and G. D. Stucky, *J. Am. Chem. Soc.*, 1998, **120**, 6024.
69 B. C. Schardt, F. J. Hollander and C. L. Hill, *J. Am. Chem. Soc.*, 1982, **104**, 3964.
70 K. Ghosh, A. A. Eroy-Reveles, M. M. Olmstead and P. K. Mascharak, *Inorg. Chem.*, 2005, **44**, 8469.
71 R. F. Ziolo, R. H. Stanford, G. R. Rossman and H. B. Gray, *J. Am. Chem. Soc.*, 1974, **96**, 7910.
72 H. Chen, J. W. Faller, R. H. Crabtree and G. W. Brudvig, *J. Am. Chem. Soc.*, 2004, **126**, 7345.